Thermoelectric transport- and Hall measurements of low defect Sb_2Te_3 thin films grown by Atomic Layer Deposition

S Zastrow[1*], J Gooth[1#], T Boehnert[1], S Heiderich[1], W Toellner[1], S Heimann[2], S Schulz[2], K Nielsch[1]

[1]Institute of Applied Physics, University of Hamburg, Jungiusstrasse 11, 20355 Hamburg, Germany

[2]Institute of Inorganic Chemistry and Center for Nanointegration Duisburg-Essen, University of Duisburg-Essen, Universitätsstrasse 5-7, 45117 Essen, Germany

Corresponding authors: [*]szastrow@physnet.uni-hamburg.de, [#]jgooth@physnet.uni-hamburg.de

Abstract

Sb_2Te_3 has recently been an object of intensive research since its promising applicability in thermoelectric, in phase-change memory devices and as a topological insulator. In this work we report highly textured Sb_2Te_3 thin films, grown by atomic layer deposition on Si/SiO_2 wafers based on the reaction of $SbCl_3$ and $Te(SiMe_3)_2$. The low deposition temperature at 80° C allows for the pre-patterning of the Sb_2Te_3 by standard lithography processes. A platform to characterize the Seebeck-coefficient S, the electrical conductivity σ as well as the Hall coefficient R_H on the same film has been developed. Comparing all temperature-dependent transport properties, three different conductive regions in the temperature range of 75 to 300 K are found. Room temperature values of S = 146 μV K^{-1}, $\sigma = 10^4$ S m^{-1} and mobility μ = 270.5 x 10^4 $m^3V^{-1}s^{-1}$ are determined. The low carrier concentration in the range of n = 2.4 x 10^{18} cm^{-3} at 300 K quantifies the low defect content of the Sb_2Te_3 thin films.

1. Introduction:

Thermoelectric and electronic properties of Sb_2Te_3 have recently generated a lot of interest for various applications. On the one hand Sb_2Te_3 is be one of the best p-type thermoelectric materials for room temperature applications, such as Peltier-elements in refrigerators, thermoelectric modules for waste heat recovery and temperature sensors [1].On the other hand Sb_2Te_3 shows a crystalline–amorphous phase transition at a temperature of around 140 °C [2], having high potential for phase change memory devices [3, 4, 5, 6, 7]. Furthermore, in-depth studies of the electronic properties of chalcogenide-based semiconductors have become a new focus due to the theoretically predicted existence of topological insulators [8]. However the supply of tellurium is very limited because of its rarity in the earth crust. Hence there is a strong need to use tellurium as efficient as possible. Nanostructured materials such as nanowires and thin films offer the possibility to cover large areas with a low amount of material. Additionally, it has been proposed that low-dimensional nanostructures may significantly enhance the efficiency of thermoelectric devices [9]. To observe the surface states of a topological insulator in transport measurements, the high surface area to volume ratio of nanostructures is promising to suppress bulk transport effects. Since controlled doping of nanostructures is still a significant challenge, the bottleneck to study topological insulator effects is to synthesize nanostructures with low carrier concentrations. Sb_2Te_3 thin films have been obtained by several growing techniques, e.g. MOCVD [10, 11], MBE [12, 13], electrochemical deposition [14, 15], coevaporation [16] and sputtering [17]. Noteworthy progress has recently been made regarding the atomic layer deposition (ALD) of Sb_2Te_3 thin films, offering the possibility to create highly defined thin layers (10 nm + number of monolayers) of ideal stoichiometric Sb_2Te_3 with a low defect concentration. However, limited publications go beyond structural characterization and focus on thermoelectric and electric transport properties. ALD of Sb_2Te_3 allows for the conformal coating of arbitrarily shaped structures with the advantages of low deposition temperatures (below 100°C) and low material consumption. Here we present thermoelectric and electronic measurements on ALD-grown Sb_2Te_3 thin films on Si/SiO_2 standard wafers. We developed a platform that allows us to characterize the Seebeck-coefficient S, the electrical conductivity σ as well as the Hall coefficient R_H of the same film over a

temperature range of 75 to 400 K. A detailed evaluation and comparison of all temperature-dependent measurements let to three different conductive regions in the Sb_2Te_3 thin film.

2. Sb_2Te_3 Film Preparation and Structural Analysis

The Sb_2Te_3 thin films were grown via atomic layer deposition (ALD) in a closed-build chamber type reactor. Silicon wafers with a top-layer of 300 nm thermal silicon oxide were used as substrate. During the whole process, the precursor materials $(Et_3Si)_2Te$ on the tellurium (Te) side and $SbCl_3$ on the antimony (Sb) side were kept at constant source temperatures of 77 °C and 55 °C, respectively. Alternate pulsing of the precursor gases into the reaction chamber leads to the formation of solid and stable Sb_2Te_3 films with subsequent elimination of Et_3SiCl (dehalosilylation reaction) during the self-limited surface reaction [5]. No film deposition could be observed below a reaction chamber temperature of 80 °C. Since the growth rate of the films strongly decreases with increasing reaction chamber temperature [3], the deposition temperature was set to 80 °C resulting in a maximal growth rate of 0.16 Å/cycle. It has been observed, that the smoothness of the Sb_2Te_3 films depends on the pulse-cycle time. Under this requirement one pulse-cycle was chosen to be 94 s, including 2 x 2 s to open the valves between the precursor bottles and the reaction chamber, 2 x 20 s of exposure time and 2 x 25 s to pump time for removal of the waste gas. Nitrogen with a continuous flow of 1.5 l/h was used as carrier gas, resulting in a base pressure of 0.1 mbar. The thickness d of the Sb_2Te_3 thin films and thus the growth rate was independently determined by X-Ray reflection (XRR) and Atomic Force Microscopy (AFM). Conventional ellipsometry could not be used to measure the film thickness due to low band gap of Sb_2Te_3 and the high reflectance of the surface. Fig. 1 (a- c) show Scanning Electron Micrographs (SEM) of Sb_2Te_3 films, deposited with different numbers of cycles, indicating a Volmer-Weber island growth mechanism. The deposited Sb_2Te_3 forms discontinuous islands, getting larger with increasing number of pulses. Above 600 pulse-cycles (d ~ 10 nm) a continuous and electrically conductive Sb_2Te_3- film was formed. The island growth mechanism imprints its structure to the surface texture and determines the roughness of the films, which leads to nanocrystalline Sb_2Te_3.

Stoichiometric analysis was performed by energy disperse X-Ray (EDX) measurements. Due to the reduced thickness, the intensity of response peaks is very low. However the EDX spectra show a Sb/Te ratio of 39.6/60.4 with estimated error of about 5 %, indicating that the stoichiometry of the deposited films is near to the ideal ratio to of 40/60. Additionally, X-ray diffraction measurements (XRD) (Cu $K\alpha_1$ - radiation) were carried out to check foreign phases and the preferential growth direction.

The XRD-spectrum in fig. 1 (d) shows mostly peaks which correspond to the (0 0 *l*) direction of the Sb_2Te_3-phase, indicating a highly textured morphology along the c-axis perpendicular to the substrate plane. This is expected from the rhombohedral crystal structure of Sb_2Te_3, where Sb and Te are alternating along the c-axis, validating the layer by layer growth mechanism of the ALD process.

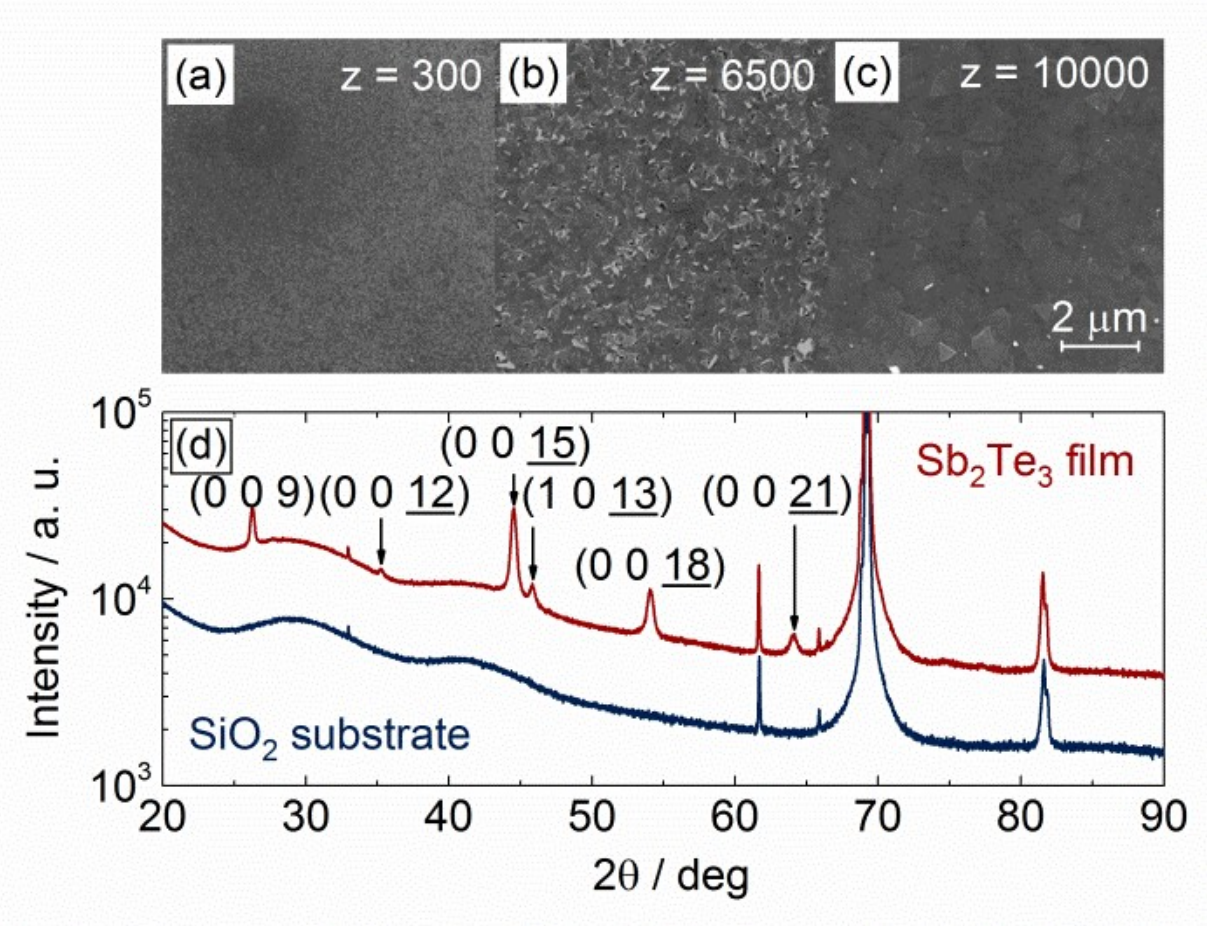

Figure 1. Scanning Electron Micrographs of the surface of ALD grown Sb_2Te_3 thin films, with 300 (a), 6500 (b) and 10000 (c) growth-cycles. X-ray diffraction pattern of the SiO_2 substrate reference (dark blue) and a 32 nm thick Sb_2Te_3 film (red) (d). The peaks correspond to literature values.

3. Device Preparation and Measurement Setup

For further characterization, the films were integrated into a specifically designed measurement platform, which combines a Hall-bar structure with resistive thermometers and a micro-heater. Due to the low deposition temperatures, the ALD process is compatible with a lithographic pre-patterning step. Therefore a soft mask for the Hall-bar was defined via common laser beam lithography using a *µPG 101* system (*Heidelberg Instruments*) with 1 µm resolution and by subsequent developing of the exposed photoresist (*ma-P 1205, Micro Resist Technology*) prior to the atomic layer deposition of Sb_2Te_3 (fig. 2 (a – c)). After lift-off in acetone (fig. 2 (d)), electrical contacts were defined in a second lithography step (fig. 2 (d)) and sputter deposition of the contact materials Ti/Pt was performed, whereby titanium served as adhesion promoter and diffusion barrier for platinum (fig. 2 (e –f)).

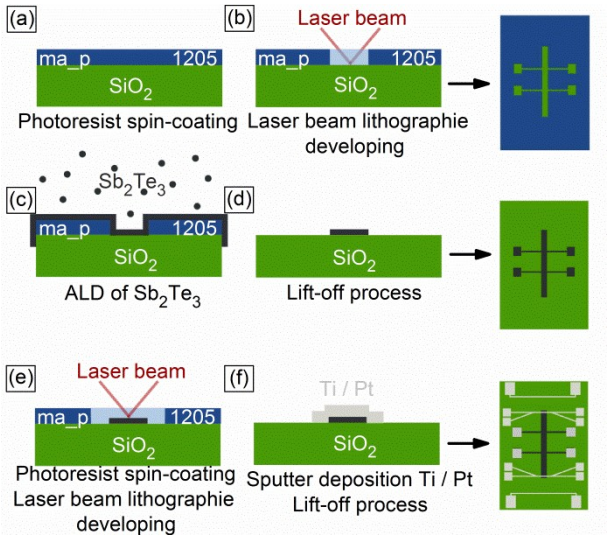

Figure 2. Illustration of the device fabrication, including two lithography patterning steps. First lithography step for pre-patterning of the Hall-bar: The Si/SiO_2 substrate is spin-coated with *maP-1205* photoresist (a). The Hall-bar structure is written by laser beam lithography and the exposed photoresist is developed subsequently (b). Sb_2Te_3 is then deposited via ALD on top of the whole substrate (c). Lift-off process in acetone. Sb_2Te_3 Hall-bar

remains (d). Second lithography step for the contact pattern on the Hall-bar (e). Sputter deposition of the metallic contact materials Ti/Pt and second lift-off process (f).

A typical device as seen in fig. 3 (a) allows in addition to four-terminal- also Hall- and Seebeck-measurements. All electrical measurements were performed in a *Versalab (Quantum Design)* equipped with a 3 T magnet and an electrical-transport measurement option (ETO) in helium atmosphere down to 75 K. The resistance of the film was determined in a four-point setup by standard lock-in technique. A current-source-meter employing an active feedback loop was chosen to work as an ideal constant current source. An AC-amplitude of 10 μA at a frequency of 6 Hz was applied between contacts I (red) and II (dark blue) and the voltage drop along the film was measured at the inner pads A and C. The IV-diagram in figure 2 (b) shows linear behavior, indicating Ohmic contacts. The Hall-resistance R_{Hall} was determined in a similar measurement configuration, but using the inner contacts A and B to measure the voltage drop across the film width, while sweeping a magnetic field from -3 to 3 T in 0.1 T steps perpendicular to the film-plane. Fig. 3 (c) shows a linear dependence of R_{Hall} as a function of magnetic field B, such that the Hall-coefficient can be calculated as $R_{\mathrm{H}} = B^{-1}\, d\, R_{\mathrm{Hall}}$. To estimate the Seebeck-coefficient S, a DC-current was applied to an on-chip heater (Fig. 3 (a)) near the film, generating a temperature gradient ΔT along the Hall-bar, which was determined by the resistivity change $\mathrm{d}R/\mathrm{d}T$ of two metallic thermometer lines I (red) and II (dark blue) located at the Hall-bar ends. For each thermometer, a four-terminal lock-in technique was used, where a sinusoidal excitation current of 1 μA was applied. The two thermometers were driven at distinct frequencies of 128.1 Hz and 186.1 Hz to avoid cross-talk and were calibrated against the substrate temperature, which was defined by the base temperature of the sample stage in the cryostat. The calibration curves (Fig. 3 (d)) show a metallic behavior. In order to calculate the Seebeck-coefficient as $S = -V_{\mathrm{th}} / \Delta T$ the assumption of a constant S within the whole film and thus a small ΔT along the Hall-bar has to be satisfied. Therefore the current through the micro-heater was chosen such that the maximum temperature gradient never exceeded 0.5 K. As an additional effect of the small temperature gradients, the cold end of the film was always kept at cryostat temperature within the minimal resolution of the four point

thermometers (10 mK), preventing an excessive rise of the average temperature in the Sb_2Te_3 film. The thermovoltage V_{th} was determined from the linear regression of the total voltage V_{total}, measured between the Hall-bar ends using one contact of each thermometer as probe while stepwise tuning the temperature gradient. This technique separates the offset-voltage V_{off} from V_{th} which add into V_{total}. The linear dependence of V_{total} from ΔT confirms that S can be assumed to be constant during the Seebeck-measurement and that the rise in the average temperature of the sample is negligibly small.

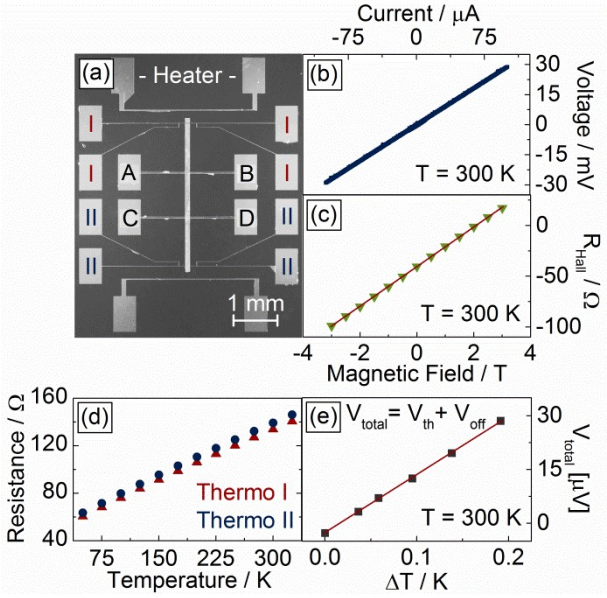

Figure 3. Micrograph of the measurement device, showing a 128 nm thick Sb_2Te_3 Hall bar with inner contacts A, B, C, D, two micro heaters, and two resistive thermometers I (red), II (blue) (a). IV curve at 300 K (b). Hall resistance R_{Hall} as a function of the magnetic field B at 300 K (c). Temperature calibration of thermometers I (red) and II (dark blue) (d). Total measured voltage V_{total} while stepwise tuning the temperature gradient ΔT, where $V_{total} = V_{th} + V_{off}$ with thermovoltage V_{th} and offset voltage V_{off}.

4. Results and Discussion

Fig. 4 (a) shows the electrical conductivity σ and the Seebeck-coefficient S of a 128 nm thick Sb_2Te_3 film (8000 ALD cycles) plotted against the temperature in the range from 75 to 400 K. The electrical conductivity decreases with increasing temperature until it saturates at the end of the measured

temperature range at 400 K. The perfect matching of up- (dark blue) and down (yellow) traces show the stability of the Sb_2Te_3 film and the reproducibility of the measurements. The Seebeck-coefficient is positive in sign over the whole temperature range, indicating hole-conduction [18]. Between 75 and 300 K the Seebeck-coefficient increases linearly with ln(T) up to a maximum of 140 µV/K at 300 K which is comparable to values reported for Sb_2Te_3 thin films in the literature [13, 19]. With further increase of the temperature, S decreases rapidly. Both, the temperature dependence of the Seebeck-coefficient and the temperature dependence of the electrical conductivity between 75 and 300 K are consistent with extrinsic semiconducting behavior [20]. For non-degenerated semiconductors with a parabolic band structure in the extrinsic range, under the assumption of a constant carrier concentration, the Seebeck-coefficient is given by [20]:

$$|S| = 3/2\ k/e\ \ln(T) + \text{const.} \qquad (1)$$

, where e is the elementary charge and k is the Boltzmann constant. Fitting the data linearly as presented here, the slope of the Seebeck-coefficient as function ln(T) differs by a factor 1/2 from 3/2 k/e. Such a deviation from the theoretical prediction has been observed by Goldsmid in 1958 for bulk Bi_2Te_3, where several possible explanations were discussed [20], e.g. the relaxation time changes with temperature, the effective masses of the charge carriers are temperature dependent or the presence of an overlapping impurity band with the conduction band. Low temperature measurements on the ALD-grown Sb_2Te_3 films show an increasing conductivity with decreasing temperature down to 10 K evidencing the presence of an overlapping impurity band. As a consequence the assumption of a non-degenerate semiconductor has to be corrected. However, in the range 75 – 300 K, where S scales linearly with ln(T), the change of the Seebeck-coefficient with temperature seems not to be dominated by the carrier concentration.

Electrical conductivity and the Seebeck-coefficient allow for the calculation of the thermoelectric power factor $S^2\sigma$, which is shown in fig. 4 (b). The temperature dependence of $S^2\sigma$ is strongly dominated by the Seebeck-coefficient, leading to a maximum of 221 µW $m^{-1}K^{-2}$ around 300 K.

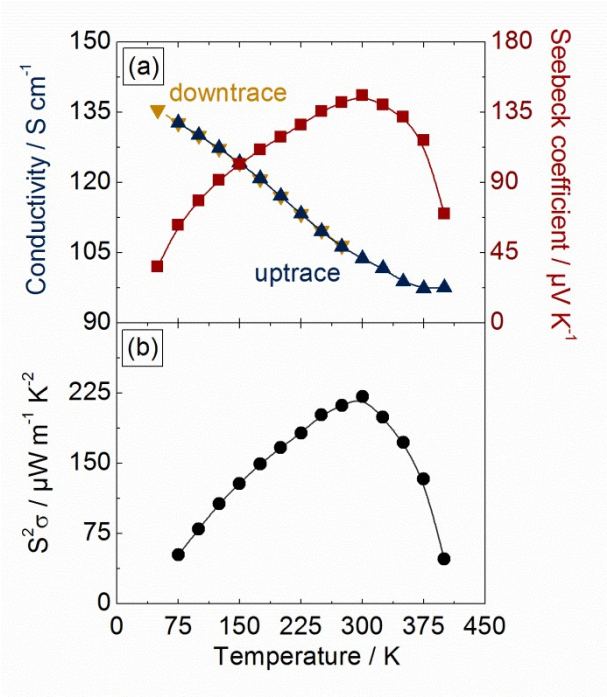

Figure 4. Electrical conductivity (blue and yellow triangles), Seebeck-coefficient (red squares) (a) and thermoelectric power factor (black dots) (b) as a function of temperature.

Fig. 5 (a) shows the results of the Hall-measurements. The Hall-coefficient R_H increases with increasing temperature, up to T = 350 K. Above, the temperature dependence changes and R_H decreases with higher temperatures. Assuming the simple formula

$$R_H[n(T)] = r/n(T)e \qquad (2)$$

where r the Hall scattering factor, to calculate the carrier concentration n, the unexpected increase of R_H with increasing temperature between 75 and 350 K would result in an unphysical decrease of the carrier concentration $n(T)$ with increasing temperature. This indicates, that the usual assumption of a constant scattering factor r = 1 has to be corrected by $r(T)$, whose temperature dependence is predominant over the dependence of n on T in $R_H(T)$ between 75 and 300 K [21]. Taking also the results of the Seebeck-analyses into account, a constant carrier concentration in this temperature regime is most likely.

Based on the Hall data, the electrical mobility μ_{nc} of the Sb_2Te_3 thin film can be calculated from the carrier concentration n and the electrical conductivity σ by the equation:

$$\mu_{nc}[\sigma(T), n(T)] = \sigma(T)\, e^{-1} n(T)^{-1}. \quad (3)$$

Fig. 5 (b) shows the mobility under two different assumptions. The green curve represents the non-corrected mobility μ_{nc}, taking the temperature dependent Hall-coefficient $R_H(T)$ into account, calculated by eq. (2). The temperature dependence of $\mu_{nc}(T)$ suggests phonon dominated scattering at high temperatures and ionized-impurity dominated scattering at low temperatures. The black curve displays the corrected mobility μ_c, calculated with a constant carrier concentration over the whole temperature range. As argued above, the analysis of the Seebeck-coefficient suggests a constant carrier concentration up to 300 K. Therefore we have fixed n, based on $R_H(T = 300\ K)$, to the value of $n(T = 300\ K) = 2.4e18\ cm^{-3}$ to calculate the corrected mobility μ_c:

$$\mu_c\,[\sigma(T), n(T = 300\ K)] = \sigma(T)\, e^{-1} n(T = 300\ K)^{-1}. \quad (4)$$

Considering the temperature dependence of μ_c, electron-phonon scattering seems to be the dominant mechanism. Note, that r at 300 K can take values between one and two, which could cause a maximum error by a factor of two in the absolute values of the electrical mobility and carrier concentration [22].

The qualitative trends of both, the non-corrected and the corrected mobility, are representative for specific temperature regimes, which can be separated in three different conductive regions:

I. Between 75 and 300 K the Sb_2Te_3 film shows extrinsic semiconducting behavior. The upper temperature limit is marked by the maximum of the Seebeck-coefficient, up to which the linear $\ln(T)$ dependence of S is valid. This dependency and the analysis of the Hall measurements, lead to the conclusions, that the carrier concentration is constant and that the transport properties are dominated by the corrected mobility μ_c (fig. 5 (b), black curve).

II. The temperature boundaries of the second region are defined by the maxima of S ($T = 300$ K) and R_H ($T = 350$ K). Here, the Seebeck-coefficient starts to decrease with increasing temperature, indicating that the thermal energy of the intrinsic carriers is high enough to overcome the band-gap of

Sb_2Te_3. Unfortunately the carrier concentration-increase cannot be calculated from Eq. (1) due to the rising Hall-coefficient. Considering the analysis of all transport measurements, no specific answer can be given, which calculated mobility is representative in this transition region.

III. Above 350 K, beyond the maximum of the R_H, the decreasing Hall-coefficient as well as the decreasing Seebeck-coefficient indicate intrinsic semiconducting behavior, which is supported by the saturating conductivity in this temperature regime. Conclusively, the carrier concentration rather increases and cannot be assumed as constant. Hence, the corrected mobility μ_c (black line), calculated with eq. (4), is no longer valid for this specific temperature regime. $n(T)$ has to be taken into account and the mobility is represented by μ_{nc} (green line).

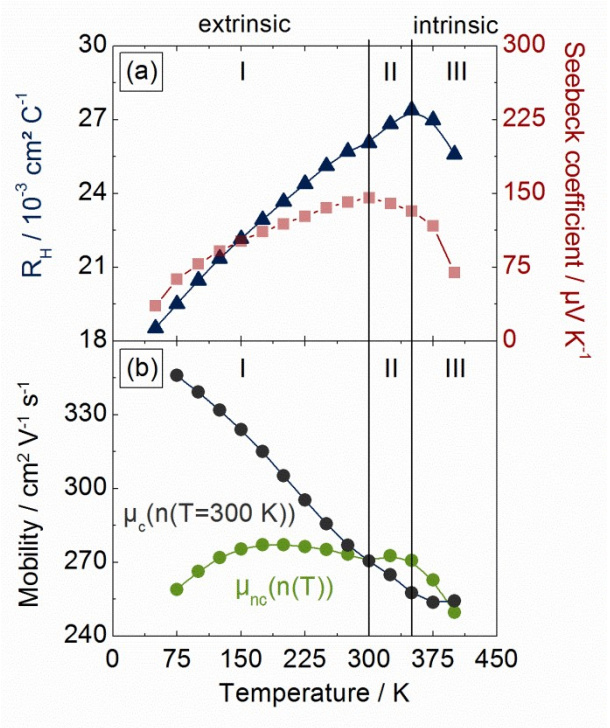

Figure 5. Hall-coefficient (blue triangles) (a), Seebeck-coefficient (red squares) (a) and electrical mobility (b) as functions of temperature. The mobilities are calculated from the temperature-dependent Hall-coefficient (green dots) and from the constant Hall-coefficient at 300 K (black dots). Three conductive regions, extrinsic region (I), transition region (II) and intrinsic region(III), are marked by black lines.

In comparison to ALD, MBE-grown epitaxial Sb_2Te_3 films exhibit similar carrier mobilities but about ten-times higher carrier densities (Table 1).Unlike MBE growth, which is performed at higher temperatures, the well-defined chemical reaction of ALD processes at relatively low temperatures leads to the formation ideal stoichiometric Sb_2Te_3 and suppresses the formation of antisite defects. A technical advantage of ALD over MBE is the absence of high-vacuum systems without losing the control about process parameters. Deposition techniques with comparable deposition pressures in the range of 0.1 mbar, such as Ion-beam sputtering (IBS) and co-evaporation show much higher carrier concentrations and lower electrical mobilities. ALD-grown films allow fundamental studies on low-defect Sb_2Te_3, without affecting the Seebeck coefficient. Although the thermoelectric performance of the ALD-grown Sb_2Te_3 thin films is suppressed by the relatively low electrical conductivity, the films could be used as well defined starting material for systematical enhancing the thermoelectric performance via nanoscale doping or structuring.

Table 1. Comparison of the Thermoelectric and transport properties of the 8000 cycle Sb_2Te_3-film at 300 K with other references. *r* is the Hall scattering factor.

deposition T (°C)	growing method	d (10^{-9}m)	σ (10^3 S/m)	S (10^{-6} V/K)	n (10^{24} m^{-3})	μ_H (10^{-4} $m^2V^{-1}s^{-1}$)	reference
400	IBS	unknown	106	106	69000	17.5	[23]
250	MBE	1000	196.6	130	26	402	[12]
230	co-evaporation	500 - 2000	66.2	140	-	-	[24]
200	MBE	250 – 350	-	78-126	7.48 - 100	20 - 279	[13]
100	ALD	128	10.4	146.0	2.4 (*r*=1)	270.5 (*r*=1)	this work

(IBS: Ion-beam sputtering deposition, MBE: Molecular beam epitaxy, ALD: Atomic layer deposition)

6. Conclusion

We have investigated measurements of the temperature-dependent Seebeck-coefficient *S*, electrical conductivity σ and Hall-coefficient R_H, of ALD-grown Sb_2Te_3 thin films deposited on non-conductive Si/SiO_2 substrates. Therefore we developed an integrated measurement platform. The low deposition

temperatures allow a pre-patterning of the films by standard laser beam lithography. Supplemental structural analysis showed, that the deposited films have a strong preferential growth direction along the c-axis (0 0 *l*). Measured values of the Seebeck-coefficient are in excellent agreement with others reported in literature and reveals that measurement platform and method are applicable. The remarkably low carrier concentrations and the high electrical mobilities clearly show the low defect content of the ALD grown Sb_2Te_3-films. This provides the possibility to observe phenomena such as the increasing Hall-coefficient with increasing temperature, which otherwise would be supressed by the high ratio of antisite defects. Evaluating and comparing all temperature-dependent measurements and by the support of theory, we found three different conductive regions in the Sb_2Te_3 thin film. The ALD technique seems to be an ideal candidate for detailed studies of complex transport mechanisms in Sb_2Te_3 thin films and can be applied to a large variety of chalcogenide-based materials. In combination with epitaxial substrates, ALD-grown Sb_2Te_3 thin films could be promising to observe surface state-dominated transport of a topological insulator.

Acknowledgements

We gratefully acknowledge financial support of the Karl-Vossloh-Stiftung and the Deutsche Forschungsgemeinschaft (DFG) via the Graduiertenkolleg 1286 "Functional Metal-Semiconductor Hybrid Systems" as well as via the SPP 1386 project "Nanostrukturierte Thermoelektrika: Theorie, Modellsysteme und kontrollierte Synthese".

References

[1] daSilva, L. W. and Kaviany, M. May 2004 *International Journal of Heat and Mass Transfer* **47(10-11)**, 2417–2435.

[2] Damodara Das, V., Soundararajan, N., and Pattabi, M. October 1987 *Journal of Materials Science* **22(10)**, 3522–3528.

[3] Pore, V., Hatanpää, T., Ritala, M., and Leskelä, M. March 2009 *Journal of the American Chemical Society* **131(10)**, 3478–3480.

[4] Hatanpaää, T., Pore, V., Ritala, M., and Leskelä, M. (2009) In ECS Transactions Vienna, Austria: . pp. 609–616.

[5] Knapas, K., Hatanpää, T., Ritala, M., and Leskelä, M. February 2010 *Chemistry of Materials* **22(4)**, 1386–1391.

[6] Pore, V., Knapas, K., Hatanpää, T., Sarnet, T., Kemell, M., Ritala, M., Leskelä, M., and Mizohata, K. January 2011 *Chemistry of Materials* **23(2)**, 247–254.

[7] Liu, B., Song, Z., Feng, S., and Chen, B. October 2005 *Microelectronic Engineering* **82(2)**, 168–174.

[8] Zhang, H., Liu, C.-X., Qi, X.-L., Dai, X., Fang, Z., and Zhang, S.-C. May 2009 *Nature Physics* **5(6)**, 438–442.

[9] Hicks, L. and Dresselhaus, M. MAY 15 1993 *Physical Review B* **47(19)**, 12727–12731.

[10] Giani, A., Boulouz, A., Pascal-Delannoy, F., Foucaran, A., Charles, E., and Boyer, A. September 1999 *Materials Science and Engineering: B* **64(1)**, 19–24.

[11] Kim, R.-Y., Kim, H.-G., and Yoon, S.-G. April 2007 *Integrated Ferroelectrics* **90(1)**, 80–87.

[12] Peranio, N., Winkler, M., Aabdin, Z., König, J., Böttner, H., and Eibl, O. February 2012 *physica status solidi (a)* **209(2)**, 289–293.

[13] Kim, Y., DiVenere, A., Wong, G. K. L., Ketterson, J. B., Cho, S., and Meyer, J. R. (2002) *Journal of Applied Physics* **91(2)**, 715.

[14] Schumacher, C., Reinsberg, K. G., Akinsinde, L., Zastrow, S., Heiderich, S., Toellner, W., Rampelberg, G., Detavernier, C., Broekaert, J. A. C., Nielsch, K., and Bachmann, J. March 2012 *Advanced Energy Materials* **2(3)**, 345–352.

[15] Leimkühler, G., Kerkamm, I., and Reineke-Koch, R. (2002) *Journal of The Electrochemical Society* **149(10)**, C474.

[16] Zou, H., Rowe, D. M., and Min, G. (2001) *Journal of Vacuum Science & Technology A: Vacuum, Surfaces, and Films* **19(3)**, 899.

[17] Chen, T., Fan, P., Zheng, Z., Zhang, D., Cai, X., Liang, G., and Cai, Z. February 2012 *Journal of Electronic Materials* **41(4)**, 679–683.

[18] Horák, J., Drašar, c., Novotný, R., Karamazov, S., and Lošťák, P. June 1995 *Physica Status Solidi (a)* **149(2)**, 549–556.

[19] Winkler, M., Liu, X., König, J. D., Buller, S., Schürmann, U., Kienle, L., Bensch, W., and Böttner, H. (2012) *Journal of Materials Chemistry* **22(22)**, 11323.

[20] Goldsmid, H. J. April 1958 *Proceedings of the Physical Society* **71(4)**, 633–646.

[21] Hung, C. and Gliessman, J. December 1954 *Physical Review* **96(5)**, 1226–1236.

[22] Jones, H. January 1951 *Physical Review* **81(1)**, 149–149.

[23] Ping, F., Zhuang-Hao, Z., Guang-Xing, L., Xing-Min, C., and Dong-Ping, Z. August 2010 *Chinese Physics Letters* **27(8)**, 087201.

[24] Goncalves, L., Couto, C., Alpuim, P., Rowe, D., and Correia, J. (2006) volume **514-516**, of MATERIALS SCIENCE FORUM : 3rd International Materials Symposium/12th Meeting of the Sociedad-Portuguesa-da-Materials (Materials 2005/SPM), Univ Aveiro, Aveiro, PORTUGAL, MAR 20-23, 2005 pp. 156–160.

DOI: 10.1088/0268-1242/28/3/035010
URN: urn:nbn:de:hbz:464-20201116-091849-9

This is the **Accepted Manuscript** version of an article accepted for publication in *Semiconductor Science and Technology 2013, 28 035010*. IOP Publishing Ltd is not responsible for any errors or omissions in this version of the manuscript or any version derived from it.
The Version of Record is available online at https://doi.org/10.1088/0268-1242/28/3/035010.